ACS APPLIED MATERIALS & INTERFACES

www.acsami.org Research Article

Propane-Trapping Ultramicroporous Metal–Organic Framework in the Low-Pressure Area toward the Purification of Propylene

Shan-Qing Yang,[‖] Fang-Zhou Sun,[‖] Rajamani Krishna, Qiang Zhang, Lei Zhou, Ying-Hui Zhang, and Tong-Liang Hu*

Cite This: *ACS Appl. Mater. Interfaces* 2021, 13, 35990–35996 Read Online

ACCESS | Metrics & More | Article Recommendations | Supporting Information

ABSTRACT: The propane (C_3H_8)-trapping adsorption behavior is considered as a potential performance to directly produce high-purity propylene (C_3H_6). Herein, we report an ultramicroporous Mn-based metal–organic framework (**NUM-7**) with a reverse C_3H_8-selective behavior in the low-pressure area. The pore structure of this material possesses more electronegative aromatic benzene rings for the stronger binding affinity to C_3H_8, and the material shows outstanding reverse ideal adsorbed solution theory (IAST) selectivity values. Single-component sorption isotherms preliminarily show the reverse adsorption behavior in the low-pressure part, and the moderate heat of adsorption further confirms this performance and exhibits less energy consumption for regeneration. In addition, the purification effect for the C_3H_8/C_3H_6 mixture is evaluated by the IAST selectivity and transient breakthrough curves, and the GCMC calculation results reveal that the fascinating C_3H_8-trapping behavior mainly depends on the multiple C–H···π interactions. Moreover, because C_3H_6 is the desired target product, the interesting C_3H_8-selective adsorption behavior of **NUM-7** may provide its potential for one-step purification of C_3H_6, and this work can provide the method of developing C_3H_8-selective materials for the purification of C_3H_6.

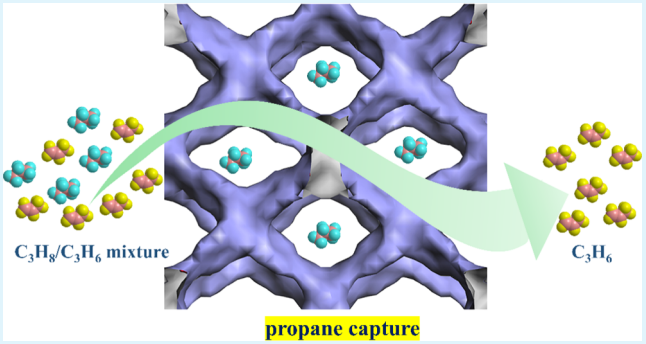

KEYWORDS: *metal–organic framework, propane selectivity, propylene purification, reverse adsorption behavior, adsorption separation*

INTRODUCTION

The separation of olefin and paraffin, listed as one of "seven chemical separations to change the world,"[1] has high commercial value as the manufacture of plastics required to produce polymer-grade pure olefins, such as ethylene and propylene. Propylene (C_3H_6), as one of the most significant raw materials in the petrochemical industry, is widely used as an important feedstock for the production of polypropylene, acrylonitrile, acroleic acid, propylene oxide, isopropanol, etc. The total global production of propylene had surpassed 120 million tons in 2016, trailing only to the production of ethylene.[2] Owing to the increase in the production of polypropylene, the worldwide demand for propylene shows an increasing trend, leading to the increasing requirements for polymer-grade (>99.5%) propylene.[3] However, the process of the production of high-purity propylene is challenging and intricate, which is related to the separation of propane from propylene raw materials. C_3H_6 is mainly produced by the steam cracking of naphtha, and most C_3H_6 is obtained from the corresponding C_3 fraction pyrolysis gas, which unavoidably mixes the impurity propane (C_3H_8). It is still a challenge to purify C_3H_6 from the C_3H_8/C_3H_6 mixture because of the similar physical properties for C_3H_6 and C_3H_8, including polarizability values (C_3H_6: 62.6 $\times$ 10^{-25} cm^3; C_3H_8: 62.9 $\times$ 10^{-25} cm^3), boiling point (C_3H_6: 225.4 K, C_3H_8: 231.1 K), and molecule size (C_3H_6: 4.16 $\times$ 4.65 $\times$ 6.44 $Å^3$; C_3H_8: 4.02 $\times$ 4.52 $\times$ 6.61 $Å^3$) (Scheme 1).[4] The traditional separation of the C_3H_8/C_3H_6 binary mixture mainly depends on the cryogenic distillation performed at low temperature (−30 °C) and high pressure (30 MPa) in a column comprising over 100 trays with a high reflux ratio because of the similar volatility of the C_3H_8/C_3H_6 mixture.[5] There is no doubt that the heat-driven process consumes more energy, entails substantial cost, and takes up enormous space.

To reduce the energy consumption and improve the separation efficiency of purifying C_3H_6, some energy-efficient, greener, and environmentally friendly advanced alternative technologies have been proposed, including the method of adsorptive separation based on a physical adsorption mechanism, such as pressure/temperature swing adsorption (PSA/TSA). It is pretty significant to search for efficient adsorbents for the process of adsorption and separation. Continuous endeavors

Received: May 27, 2021
Accepted: July 7, 2021
Published: July 21, 2021

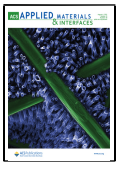

https://doi.org/10.1021/acsami.1c09808
ACS Appl. Mater. Interfaces 2021, 13, 35990–35996

Scheme 1. Molecular Structure and Physical Properties of Propane and Propylene (b.p. = Boiling Point)

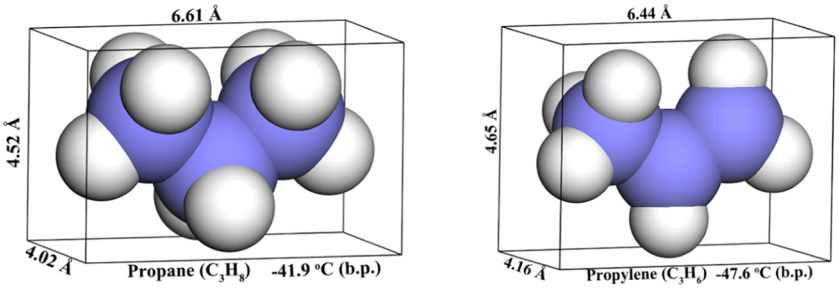

Kinetic diameter difference: < 0.5 Å; b.p. (boiling point) difference: < 6 °C

have been devoted to developing more suitable adsorbents for the purification of C_3H_6, such as zeolites,[6−8] carbon molecular sieves,[9] and silica gel.[10] Nevertheless, these materials still cannot meet the polymer-grade requirements for practical industrial application, and thus researchers are still struggling to search for ideal adsorbents.

Metal−organic frameworks (MOFs), or porous coordination polymers (PCPs), as a class of novel crystalline porous solid materials,[11−13] with metal or metal cluster node and organic linker, have been developed as adsorbents for the separation of hydrocarbons such as C_2H_2/C_2H_4,[14−17] C_2H_6/C_2H_4,[18,19] $C_2H_6/C_2H_4/C_2H_2$,[20−24] C_3H_6/C_3H_4,[25,26] and C_3H_8/C_3H_6[27,28] on the basis of their typical characteristics of the designable and modifiable structure, pore size tunability and controllability, and relatively large specific surface area and porosity. In light of the fascinating structure feature of the MOF material, it has been demonstrated to overcome the limitations of traditional porous solid materials and is widely used in the application of gas adsorption and separation. Generally, MOFs as a kind of adsorbent could distinguish the gas molecules with respect to the size, shape, and polarity based on the mechanism of thermodynamic, kinetic, and molecule size sieving. At present, the majority of adsorbents preferentially adsorb C_3H_6 molecules in the C_3H_6/C_3H_8 mixture, and the C=C bond in C_3H_6 provides an unambiguous recognition to MOFs with unsaturated metal ions to form a strong host−guest interaction.[29] In addition, the separation based on the molecule size sieving mechanism or the kinetically driven behavior frequently provides C_3H_6-selective MOFs due to the comparatively larger gas size of C_3H_8 than that of C_3H_6.[30,31] However, because the desired product is C_3H_6, the C_3H_6-selective MOFs are confronted with a desorption process that increases the energy consumption and operation steps. Nowadays, it is expected to develop C_3H_8-selective materials so that the separation process could be simplified and save energy for extra desorption. Compared with the difference in the molecular structure between C_2H_6/C_2H_4, the difference between C_3H_8 and C_3H_6 is relatively small because they all have the same alkyl part (i.e., $-CH_3$ group). Therefore, there are great challenges on the development of C_3H_8-selective materials. To date, the C_3H_8-selective MOFs for the purification of C_3H_6 have still rarely been reported.[32−34]

Herein, we report a robust ultramicroporous Mn-based metal−organic framework **NUM-7** with more nonpolar aromatic rings decorating the channels, recently reported by our group,[23] as a propane-selective material for propane/propylene separation. The pore structure environment of **NUM-7** is suitable to selectively adsorb C_3H_8, which may provide its potential for one-step purification of C_3H_6. The single-component gas adsorption isotherms indicate that **NUM-7a** (activated **NUM-7**) preferentially adsorbs C_3H_8 in the C_3H_8/C_3H_6 mixture, and the heat of adsorption comprehensively affirms this view. The ideal adsorbed solution theory (IAST) selectivity calculations and the transient breakthrough experiments were carried out to evaluate the practical separation performance. Furthermore, the reverse adsorption of strong binding affinity for C_3H_8 was validated by Grand Canonical Monte Carlo (GCMC) calculations. The Mn-MOF of reverse behavior of preferentially capturing C_3H_8 makes it a practical prospective adsorbent for the challenging C_3H_8/C_3H_6 separation.

EXPERIMENTAL SECTION

Materials. All of the chemicals and reagents were received from commercial suppliers and used without further purification. Liquid nitrogen, propane (99.99%), and propylene (99.99%) were provided from Air Liquid China.

Synthesis of Materials. The Mn-based MOF was prepared according to our recent work with slight modifications.[23] In a typical process, a mixture of $MnCl_2{\cdot}4H_2O$ (2 mmol, 0.40 g) and H_4TCPE (0.2 mmol, 0.20 g), dimethylformamide (DMF) (30 mL), CH_3CN (20 mL), and deionized water (5 mL) was placed in 100 mL beaker with ultrasonic dispersion at room temperature for 10 min. Then, it was divided into multiple 10 mL screw-capped glass vials and heated at 358 K for 48 h and naturally cooled to room temperature. The resulting yellow stick crystals were obtained and washed with DMF until impurities were removed and then dried in the atmosphere of air.

The as-synthesized **NUM-7** sample was washed several times with DMF, then the fresh sample was guest exchanged with anhydrous methanol for 6 h, and the solvent-exchange sample was evacuated under vacuum conditions (less than 10^{-5} Torr) at 423 K for 10 h to obtain activated **NUM-7** (**NUM-7a**).

Characterization. Powder X-ray diffraction (PXRD) data were gathered on Rigaku Miniflex 600 at 40 kV and 15 mA using Cu Kα radiation in the air atmosphere at a scan rate of 5.0° min^{-1}.

Gas Adsorption Measurements. The single-component gas adsorption isotherms of propane and propylene were carried out on a Micromeritics ASAP 2020 adsorption apparatus at different temperatures (273, 298, 313 K). All of the gases used were of 99.99% purity. The free space of the system was determined using helium gas. Before each measurement, the as-synthesized sample was in situ degassed under a high vacuum at test temperature for 3 h.

Grand Canonical Monte Carlo (GCMC) Calculations. The GCMC simulations were carried out for the adsorption of C_3H_8 and C_3H_6 in **NUM-7a**. The skeleton of **NUM-7a** and gas molecules were regarded as rigid bodies. The optimal adsorption sites were simulated under 298 K and 1.0 bar by the fixed loading task and the Metropolis method. The loading steps, equilibration steps, and the production steps were all set to 2.0×10^7. The gas−skeleton interaction and the gas−gas interaction were characterized by the standard universal force field (UFF). The atomic partial charges of the host skeleton of **NUM-7a**

https://doi.org/10.1021/acsami.1c09808
ACS Appl. Mater. Interfaces 2021, 13, 35990−35996

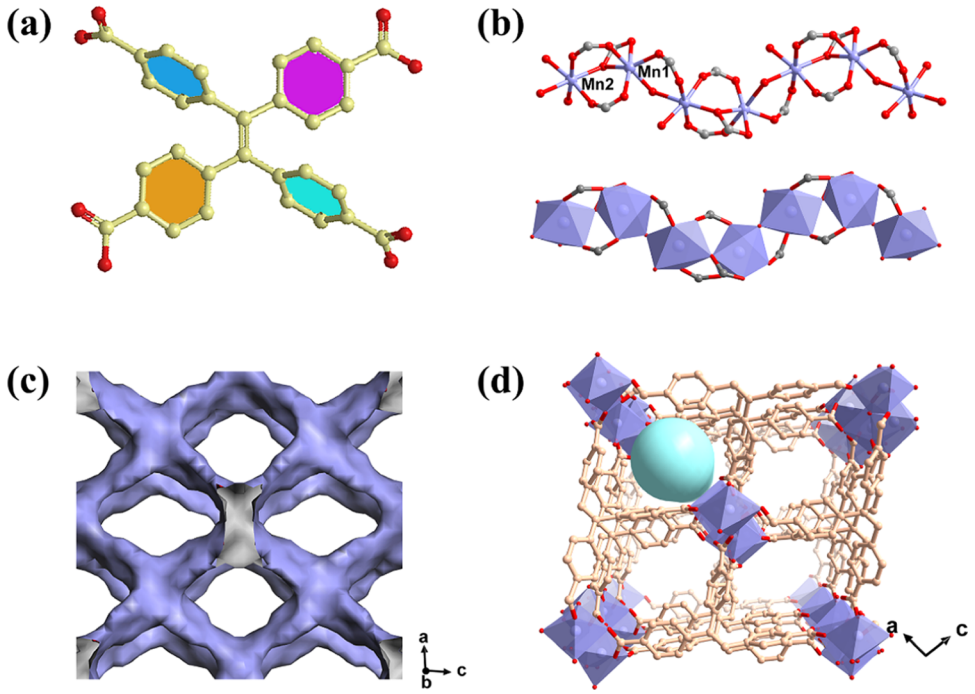

Figure 1. (a) Structure of H_4TCPE ligand for the construction of **NUM-7**. (b) Infinitely extended Mn−O chain SBU of the **NUM-7** framework. (c) Channels of **NUM-7** framework. (d) Three-dimensional framework of **NUM-7** viewed along the *b*-axis.

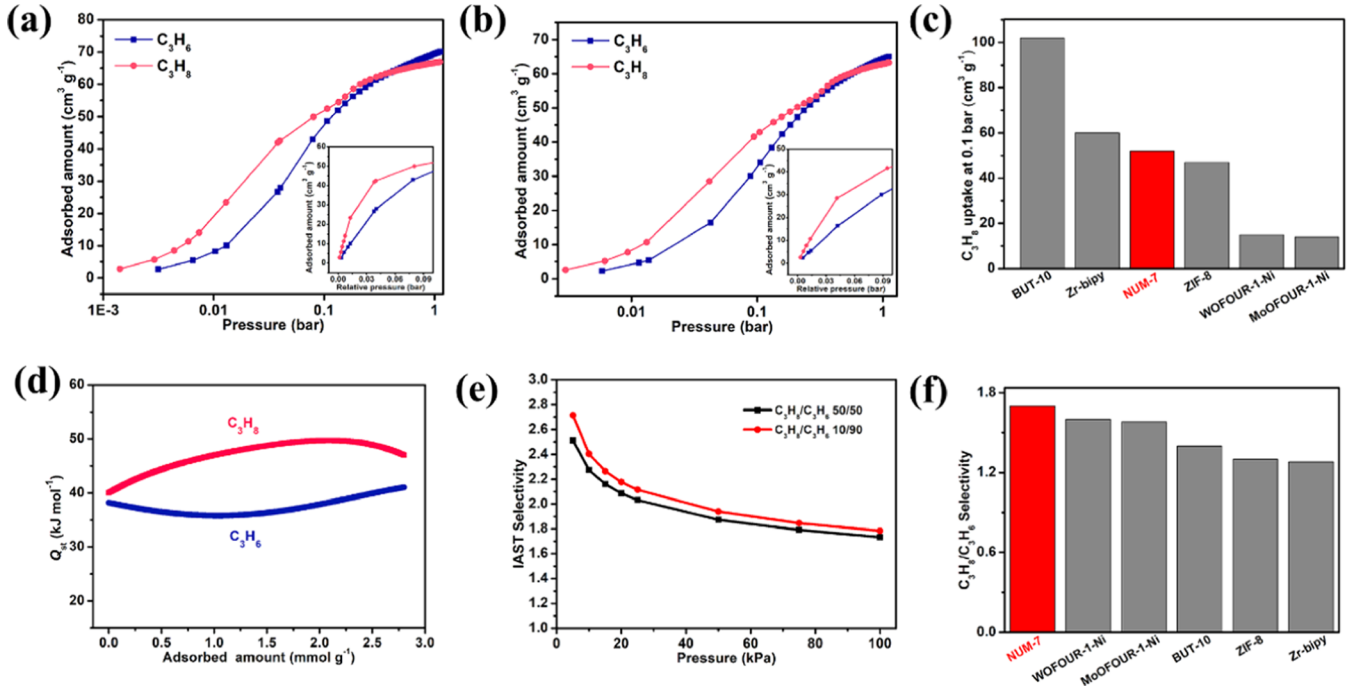

Figure 2. (a, b) Adsorption isotherms of propane and propylene on **NUM-7a** at 298 and 313 K and 1.0 bar. (c) Comparison of the C_3H_8 uptake observed at 0.1 bar. (d) Adsorption heat enthalpy of C_3H_8 and C_3H_6, calculated from the single-component C_3H_8 and C_3H_6 adsorption data at 298 and 313 K. (e) Predicted mixture selectivity of **NUM-7a** by the IAST method for C_3H_8/C_3H_6 (black: 50/50, red: 10/90, respectively) mixture at 298 K. (f) Comparison of the IAST selectivity obtained for C_3H_8/C_3H_6 using the C_3H_8-selective MOFs at 298 K and 1.0 bar.

were used for the Qeq method. The cutoff radius used for the Lennard-Jones interactions is 18.5 Å.[35,36]

RESULTS AND DISCUSSION

The as-synthesized sample was obtained using the solvothermal method with H_4TCPE and $MnCl_2$ in a mixture of DMF, CH_3CN, and deionized water under 358 K for 48 h. Also, the phase purity was proved by contrasting the experimental PXRD pattern with the corresponding simulated one derived from the single-crystal structure (Figure S1). In the Mn-based MOF structure, the tetracarboxylic acid H_4TCPE with multi-coordination is an organic linker, and the infinitely extending Mn−O chain SBU composed of dual-core SBU is an inorganic building unit. The organic ligands and inorganic metal clusters

https://doi.org/10.1021/acsami.1c09808
ACS Appl. Mater. Interfaces 2021, 13, 35990−35996

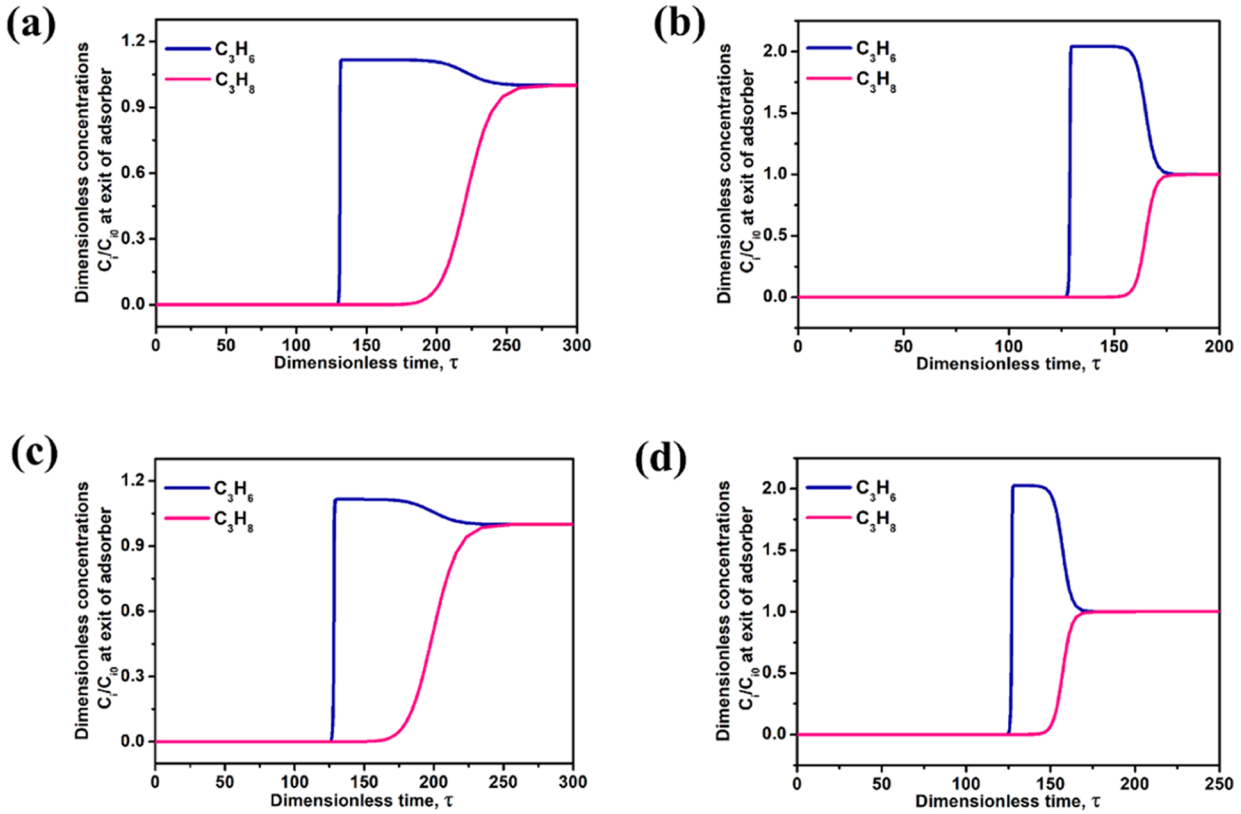

Figure 3. Transient breakthrough simulations of C_3H_8/C_3H_6 (10/90 and 50/50, v/v) binary mixture in an adsorber bed packed using **NUM-7a**. Different operating conditions were (a) C_3H_8/C_3H_6 (10/90, v/v) at 298 K; (b) C_3H_8/C_3H_6 (50/50, v/v) at 298 K; (c) C_3H_8/C_3H_6 (10/90, v/v) at 313 K; and (d) C_3H_8/C_3H_6 (50/50, v/v) at 313 K. The total bulk gas phase in the fixed bed is 100 kPa.

form a three-dimensional skeleton, which generates a one-dimensional channel with a pore size of approximately 4.7 × 7.8 Å^2 along the *b*-axis (Figure 1c,d). The accessible channel surfaces are surrounded by a low-polarity benzene ring to afford intensive electronegative binding sites, offering multiple fascinating binding affinity potentials to paraffin. This point has been proved to be beneficial to the adsorption of paraffin than olefin, such as C_2H_6/C_2H_4 separation. This interesting adsorption behavior of C_2 hydrocarbons prompted us to explore its performance to adsorb and separate C_3H_8/C_3H_6.

The available pore surface of **NUM-7a** is affluent in the phenyl rings of organic ligands; therefore, this inert microporous structure is particularly suitable to preferentially adsorb larger polarizability ethane.[23] Inspired by the reverse adsorption phenomenon of C_2 hydrocarbons, the adsorption isotherms of C_3H_8 and C_3H_6 were carried out. Hence, low-pressure C_3H_8 and C_3H_6 sorption isotherms data under ambient conditions were collected on **NUM-7a** (Figure 2a,b), with the adsorption capacity of 66.7 cm^3 g^{-1} for C_3H_8 and 69.4 cm^3 g^{-1} for C_3H_6 at 298 K and 1.0 bar. At 298 K, the C_3H_8 adsorption capacity of **NUM-7a** (2.98 mmol g^{-1}) is higher than that of MAF-23-O (1.17 mmol g^{-1}),[37] WOFOUR-1-Ni (0.6 mmol g^{-1}), and MoFOUR-1-Ni (0.7 mmol g^{-1}).[33] The attracting section is that we found analogous reverse adsorption behavior that C_3H_8 adsorption isotherm shows a remarkably steeper and higher adsorption tendency than that of C_3H_6 at the low-pressure area (Figure 2a,b), implying the stronger host−guest interaction between C_3H_8 and the framework of **NUM-7a** compared with that of C_3H_6. The C_3H_8 adsorption amount reached approximately 25 cm^3 g^{-1} under 0.015 bar; apparently, the value is more than twice that of C_3H_6 (12 cm^3 g^{-1}). In addition, the calculated Henry selectivity value can be up to 2.75 under low pressure (Figures 1c, S2, and S3). The adsorption phenomenon exhibited that the material showed a stronger binding affinity to C_3H_8 and preliminarily verified the potential of **NUM-7a** in the one-step purification of C_3H_6.

To make a quantitative comparison of the host−guest binding affinity between the guest gas molecules and the host framework of **NUM-7a**, coverage-dependent adsorption enthalpies (Q_{st}) of **NUM-7a** for C_3H_8 and C_3H_6 were established experimentally from single-component isotherms collected at 298 and 313 K using the virial equation. As shown in Figure 2d, the resultant Q_{st} for C_3H_8 at the near-zero coverage is 40.03 kJ mol^{-1}, which indeed is higher than that of 38.19 kJ mol^{-1} for C_3H_6. This result indicates that **NUM-7a** has a stronger binding affinity for C_3H_8 than that for C_3H_6, which is adequately consistent with the gas adsorption isotherms results and proves the feasibility of the C_3H_8 preferential adsorption in the framework. Moreover, the Q_{st} value of C_3H_8 for **NUM-7a** (40.03 kJ mol^{-1}) is lower than that of WOFOUR-1-Ni (42 kJ mol^{-1}),[33] MAF-23 (42 kJ mol^{-1}),[37] and NKU-FlexMOF-1a (52 kJ mol^{-1}),[28] indicating the less energy consumption for the adsorbent regeneration.

Motivated by the behavior of preferentially adsorbing C_3H_8 molecules, the adsorption selectivity calculation was carried out based on the ideal adsorbed solution theory (IAST), which can quantitatively evaluate the separation potential of **NUM-7a** for the removal of C_3H_8 from the C_3H_8/C_3H_6 binary mixture. As shown in Figure 2e, the calculated C_3H_8/C_3H_6 (50/50) mixture selectivity value of **NUM-7a** exceeds 2.2 below 0.1 bar at 298 K. In addition, the selectivity still maintains above 1.7 in a wide pressure range, implying the C_3H_8/C_3H_6 separation potential. Furthermore, the selectivity value for the C_3H_8/C_3H_6 (10/90,

https://doi.org/10.1021/acsami.1c09808
ACS Appl. Mater. Interfaces 2021, 13, 35990−35996

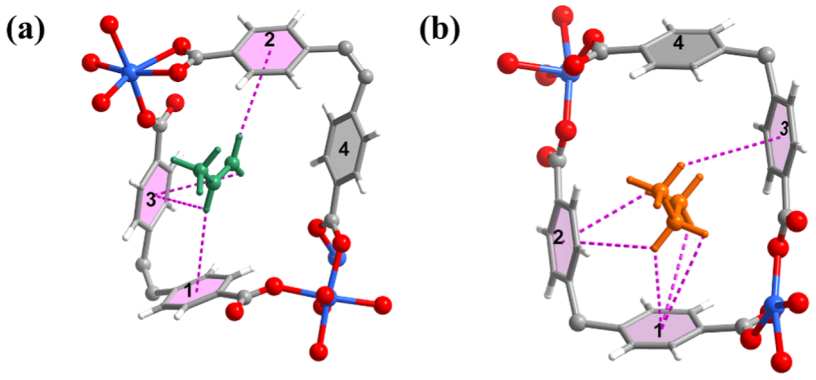

Figure 4. Preferential binding sites for (a) C_3H_6 and (b) C_3H_8 molecules and the distance of guest molecule contacts within the cavity of aromatic benzene rings (numbered as 1−4). The C−H···π interactions are highlighted as pink dashed lines.

v/v) mixture, close to the actual mixture component, is around 1.8 to 2.7 in a wide pressure range. The selectivity values are comparable to WOFOUR-1-Ni (1.6) and higher than that of MoFOUR-1-Ni (1.58), BUT-10 (1.4), and ZIF-8 (1.3).[32−34]

To evaluate the feasibility of C_3H_8/C_3H_6 binary mixture separation on the material of **NUM-7a**, transient breakthrough simulations were carried out for the separation of 10/90 and 50/50 (C_3H_8/C_3H_6, v/v) at 298 and 313 K. Figure 3a−d exhibits the outlet concentrations of C_3H_8/C_3H_6 existing in the fixed bed of adsorber packed with **NUM-7a** as a function of dimensionless time, τ, at 298 and 313 K and 1.0 bar. Particularly, benefiting from the high C_3H_8 adsorption uptake and high C_3H_8/C_3H_6 selectivity at a low-pressure area, **NUM-7a** showed good separation ability. Indeed, C_3H_6 was first eluted through the fixed bed, while C_3H_8 was still adsorbed; the behavior indicated that the adsorbent **NUM-7a** possessed the capacity of one-step green and efficient purification of C_3H_6.

To structurally understand the interesting gas adsorption behavior of the preferential C_3H_8 adsorbed within **NUM-7**, GCMC calculations were carried out on the framework. As shown in Figure 4, in **NUM-7a**, the C_3H_8 molecule interacts with three benzene rings originating from three adjacent rings to form six C−H···π interactions (C−H···π 2.784(1)−3.868(1) Å), which are comparable with the sum of the van der Waals radii of hydrogen/carbon (1.20/1.70 Å) and carbon (1.70 Å) atoms. By comparison, there are only four C−H···π interactions (C−H···π 3.489(0) − 3.929(1) Å) formed by the C_3H_6 molecule with three benzene rings. Therefore, C_3H_8 interacts more strongly with the skeleton than C_3H_6, mainly owing to the larger molecule size, more complex molecular configurations, and more number of multiple weak C−H···π interactions. This result is consistent with the Q_{st} values and the low-pressure area of the single adsorption isotherm.

CONCLUSIONS

In summary, by virtue of the surface functionalities with low-polarity benzene rings of MOF materials, intricate and reverse gas adsorption of different complicacies could be achieved. For the more difficult C_3H_8/C_3H_6 mixture separation, the above results illustrate that **NUM-7a** shows strong binding affinities to C_3H_8 compared with C_3H_6. The preferential trapping of C_3H_8 over C_3H_6 realizes the reverse adsorption, this performance of preferential adsorption C_3H_8 from the C_3H_8/C_3H_6 mixture is beneficial as a one-step greener C_3H_6 purification, achieving the target of energy efficiency and reasonable use of space. Additionally, the moderate adsorption enthalpies could reduce the energy consumption for the regeneration process. This investigation reveals the tactics to design such paraffin-selective materials and promote the C_3H_8-selective material development. Overall, the incessant exploration endeavor of searching efficient adsorbents for advanced adsorption separation technology would provide tremendous energy benefits.

ASSOCIATED CONTENT

Supporting Information

The Supporting Information is available free of charge at https://pubs.acs.org/doi/10.1021/acsami.1c09808.

Experimental sections, including PXRD patterns, breakthrough simulations, and energy distributions in **NUM-7a** (PDF)

AUTHOR INFORMATION

Corresponding Author

Tong-Liang Hu − *School of Materials Science and Engineering, National Institute for Advanced Materials, Nankai University, Tianjin 300350, China; State Key Laboratory of Coordination Chemistry, Nanjing University, Nanjing 210023, China;* orcid.org/0000-0001-9619-9867; Email: tlhu@nankai.edu.cn

Authors

Shan-Qing Yang − *School of Materials Science and Engineering, National Institute for Advanced Materials, Nankai University, Tianjin 300350, China*

Fang-Zhou Sun − *School of Materials Science and Engineering, National Institute for Advanced Materials, Nankai University, Tianjin 300350, China*

Rajamani Krishna − *Van 't Hoff Institute for Molecular Sciences, University of Amsterdam, 1098 XH Amsterdam, The Netherlands;* orcid.org/0000-0002-4784-8530

Qiang Zhang − *School of Materials Science and Engineering, National Institute for Advanced Materials, Nankai University, Tianjin 300350, China*

Lei Zhou − *School of Materials Science and Engineering, National Institute for Advanced Materials, Nankai University, Tianjin 300350, China*

Ying-Hui Zhang − *School of Materials Science and Engineering, National Institute for Advanced Materials, Nankai University, Tianjin 300350, China*

Complete contact information is available at: https://pubs.acs.org/10.1021/acsami.1c09808

Author Contributions

[‖]S.-Q.Y. and F.-Z.S. contributed equally to this work.

Notes

The authors declare no competing financial interest.

■ ACKNOWLEDGMENTS

This work was financially supported by the Natural Science Foundation of Tianjin (20JCYBJC01330), the National Natural Science Foundation of China (21673120), and the Fundamental Research Funds for the Central Universities, Nankai University (63211040).

■ REFERENCES

(1) Sholl, D. S.; Lively, R. P. Seven Chemical Separations to Change the World. *Nature* **2016**, *532*, 435−437.
(2) Cadiau, A.; Adil, K.; Bhatt, P. M.; Belmabkhout, Y.; Eddaoudi, M. A Metal-Organic Framework-Based Splitter for Separating Propylene from Propane. *Science* **2016**, *353*, 137−140.
(3) Martins, V. F.; Ribeiro, A. M.; Plaza, M. G.; Santos, J. C.; Loureiro, J. M.; Ferreira, A. F.; Rodrigues, A. E. Gas-Phase Simulated Moving Bed: Propane/Propylene Separation on 13X Zeolite. *J. Chromatogr. A* **2015**, *1423*, 136−148.
(4) Ding, Q.; Zhang, Z.; Yu, C.; Zhang, P.; Wang, J.; Kong, L.; Cui, X.; He, C.-H.; Deng, S.; Xing, H. Separation of Propylene and Propane with a Microporous Metal-Organic Framework via Equilibrium-Kinetic Synergetic Effect. *AIChE J.* **2021**, *67*, No. e17094.
(5) Rege, S. U.; Yang, R. T. Propane/Propylene Separation by Pressure Swing Adsorption: Sorbent Comparison and Multiplicity of Cyclic Steady States. *Chem. Eng. Sci.* **2002**, *57*, 1139−1149.
(6) Grande, C. A.; Rodrigues, A. E. Propane/Propylene Separation by Pressure Swing Adsorption Using Zeolite 4A. *Ind. Eng. Chem. Res.* **2005**, *44*, 8815−8829.
(7) Da Silva, F. A.; Rodrigues, A. E. Vacuum Swing Adsorption for Propylene/Propane Separation with 4A Zeolite. *Ind. Eng. Chem. Res.* **2001**, *40*, 5758−5774.
(8) Grande, C. A.; Poplow, F.; Rodrigues, A. E. Technology, Vacuum Pressure Swing Adsorption to Produce Polymer-Grade Propylene. *Sep. Sci. Technol.* **2010**, *45*, 1252−1259.
(9) Ma, X.; Williams, S.; Wei, X.; Kniep, J.; Lin, Y. Propylene/Propane Mixture Separation Characteristics and Stability of Carbon Molecular Sieve Membranes. *Ind. Eng. Chem. Res.* **2015**, *54*, 9824−9831.
(10) Grande, C. A.; Rodrigues, A. E. Adsorption Equilibria and Kinetics of Propane and Propylene in Silica Gel. *Ind. Eng. Chem. Res.* **2001**, *40*, 1686−1693.
(11) Furukawa, H.; Cordova, K. E.; O'Keeffe, M.; Yaghi, O. M. The Chemistry and Applications of Metal-Organic Frameworks. *Science* **2013**, *341*, No. 1230444.
(12) Yaghi, O. M.; O'Keeffe, M.; Ockwig, N. W.; Chae, H. K.; Eddaoudi, M.; Kim, J. Reticular Synthesis and the Design of New Materials. *Nature* **2003**, *423*, 705−714.
(13) Cui, W.-G.; Hu, T.-L.; Bu, X.-H. Metal-Organic Framework Materials for the Separation and Purification of Light Hydrocarbons. *Adv. Mater.* **2020**, *32*, No. 1806445.
(14) Zhang, Z.; Peh, S. B.; Wang, Y.; Kang, C.; Fan, W.; Zhao, D. Efficient Trapping of Trace Acetylene from Ethylene in an Ultramicroporous Metal-Organic Framework via Synergistic Effect of High-Density Open Metal Sites and Electronegative Sites. *Angew. Chem., Int. Ed.* **2020**, *59*, 18927−18932.
(15) Peng, Y.-L.; Pham, T.; Li, P.; Wang, T.; Chen, Y.; Chen, K.-J.; Forrest, K. A.; Space, B.; Cheng, P.; Zaworotko, M. J.; Zhang, Z. Robust Ultramicroporous Metal-Organic Frameworks with Benchmark Affinity for Acetylene. *Angew. Chem., Int. Ed.* **2018**, *57*, 10971−10975.
(16) Hu, T.-L.; Wang, H.; Li, B.; Krishna, R.; Wu, H.; Zhou, W.; Zhao, Y.; Han, Y.; Wang, X.; Zhu, W.; Yao, Z.; Xiang, S.; Chen, B. Microporous Metal-Organic Framework with Dual Functionalities for Highly Efficient Removal of Acetylene from Ethylene/Acetylene Mixtures. *Nat. Commun.* **2015**, *6*, No. 7328.
(17) Jiang, L.; Tian, Y.; Sun, T.; Zhu, Y.; Ren, H.; Zou, X.; Ma, Y.; Meihaus, K. R.; Long, J. R.; Zhu, G. A Crystalline Polyimide Porous Organic Framework for Selective Adsorption of Acetylene over Ethylene. *J. Am. Chem, Soc.* **2018**, *140*, 15724−15730.
(18) Pei, J.; Wang, J.-X.; Shao, K.; Yu, Y.; Cui, Y.; Wu, H.; Zhou, W.; Li, B.; Qian, G. Engineering Microporous Ethane-Trapping Metal-Organic Frameworks for Boosting Ethane/Ethylene Separation. *J. Mater. Chem. A* **2020**, *8*, 3613−3620.
(19) Qazvini, O. T.; Babarao, R.; Shi, Z.-L.; Zhang, Y.-B.; Telfer, S. G. A Robust Ethane-Trapping Metal-Organic Framework with a High Capacity for Ethylene Purification. *J. Am. Chem. Soc.* **2019**, *141*, 5014−5020.
(20) Xu, Z.; Xiong, X.; Xiong, J.; Krishna, R.; Li, L.; Fan, Y.; Luo, F.; Chen, B. A Robust Th-azole Framework for Highly Efficient Purification of C_2H_4 from a $C_2H_4/C_2H_2/C_2H_6$ Mixture. *Nat. Commun.* **2020**, *11*, No. 3163.
(21) Zeng, H.; Xie, X. J.; Xie, M.; Huang, Y. L.; Luo, D.; Wang, T.; Zhao, Y.; Lu, W.; Li, D. A Cage-Interconnected Metal-Organic Framework with Tailored Apertures for Efficient C_2H_6/C_2H_4 Separation under Humid Conditions. *J. Am. Chem. Soc.* **2019**, *141*, 20390−20396.
(22) Hao, H.-G.; Zhao, Y.-F.; Chen, D.-M.; Yu, J.-M.; Tan, K.; Ma, S.; Chabal, Y.; Zhang, Z.-M.; Dou, J.-M.; Xiao, Z.-H.; Day, G.; Zhou, H.-C.; Lu, T.-B. Simultaneous Trapping of C_2H_2 and C_2H_6 from a Ternary Mixture of $C_2H_2/C_2H_4/C_2H_6$ in a Robust Metal-Organic Framework for the Purification of C_2H_4. *Angew. Chem., Int. Ed.* **2018**, *57*, 16067−16071.
(23) Sun, F.-Z.; Yang, S.-Q.; Krishna, R.; Zhang, Y.-H.; Xia, Y.-P.; Hu, T.-L. Microporous Metal−Organic Framework with a Completely Reversed Adsorption Relationship for C_2 Hydrocarbons at Room Temperature. *ACS Appl. Mater. Interfaces* **2020**, *12*, 6105−6111.
(24) Yang, S.-Q.; Sun, F.-Z.; Liu, P.; Li, L.; Krishna, R.; Zhang, Y.-H.; Li, Q.; Zhou, L.; Hu, T.-L. Efficient Purification of Ethylene from C_2 Hydrocarbons with an C_2H_6/C_2H_2-Selective Metal-Organic Framework. *ACS Appl. Mater. Interfaces* **2021**, *13*, 962−969.
(25) Xu, M.-M.; Kong, X.-J.; He, T.; Wu, X.-Q.; Xie, L.-H.; Li, J.-R. Reaction Duration-Dependent Formation of Two Cu(II)-MOFs with Selective Adsorption Properties of C_3H_4 over C_3H_6. *Dalton Trans.* **2019**, *48*, 9225−9233.
(26) Li, L.; Lin, R.-B.; Krishna, R.; Wang, X.; Li, B.; Wu, H.; Li, J.; Zhou, W.; Chen, B. Flexible-Robust Metal-Organic Framework for Efficient Removal of Propyne from Propylene. *J. Am. Chem. Soc.* **2017**, *139*, 7733−7736.
(27) Geier, S. J.; Mason, J. A.; Bloch, E. D.; Queen, W. L.; Hudson, M. R.; Brown, C. M.; Long, J. R. Selective Adsorption of Ethylene over Ethane and Propylene over Propane in the Metal−Organic Frameworks M_2(dobdc) (M = Mg, Mn, Fe, Co, Ni, Zn). *Chem. Sci.* **2013**, *4*, 2054−2061.
(28) Yu, M.-H.; Space, B.; Franz, D.; Zhou, W.; He, C.; Li, L.; Krishna, R.; Chang, Z.; Li, W.; Hu, T.-L.; Bu, X.-H. Enhanced Gas Uptake in a Microporous Metal-Organic Framework via a Sorbate Induced-Fit Mechanism. *J. Am. Chem. Soc.* **2019**, *141*, 17703−17712.
(29) Bloch, E. D.; Queen, W. L.; Krishna, R.; Zadrozny, J. M.; Brown, C. M.; Long, J. R. Hydrocarbon Separations in a Metal-Organic Framework with Open Iron(II) Coordination Sites. *Science* **2012**, *335*, 1606−1610.
(30) Li, K.; Olson, D. H.; Seidel, J.; Emge, T. J.; Gong, H.; Zeng, H.; Li, J. Zeolitic Imidazolate Frameworks for Kinetic Separation of Propane and Propene. *J. Am. Chem. Soc.* **2009**, *131*, 10368−10369.
(31) Cui, X.; Chen, K.; Xing, H.; Yang, Q.; Krishna, R.; Bao, Z.; Wu, H.; Zhou, W.; Dong, X.; Han, Y.; Li, B.; Ren, Q.; Zaworotko, M. J.; Chen, B. Pore Chemistry and Size Control in Hybrid Porous Materials for Acetylene Capture from Ethylene. *Science* **2016**, *353*, 141−144.
(32) Böhme, U.; Barth, B.; Paula, C.; Kuhnt, A.; Schwieger, W.; Mundstock, A.; Caro, J.; Hartmann, M. Ethene/Ethane and Propene/Propane Separation via the Olefin and Paraffin Selective Metal-Organic Framework Adsorbents CPO-27 and ZIF-8. *Langmuir* **2013**, *29*, 8592−8600.

https://doi.org/10.1021/acsami.1c09808
ACS Appl. Mater. Interfaces 2021, 13, 35990−35996

(33) Yang, L.; Cui, X.; Ding, Q.; Wang, Q.; Jin, A.; Ge, L.; Xing, H. Polycatenated Molecular Cage-Based Propane Trap for Propylene Purification with Recorded Selectivity. *ACS Appl. Mater. Interfaces* **2020**, *12*, 2525−2530.
(34) He, C.; Wang, Y.; Chen, Y.; Wang, X.; Yang, J.; Li, L.; Li, J. Modification of the Pore Environment in UiO-type Metal-Organic Framework toward Boosting the Separation of Propane/Propylene. *Chem. Eng. J.* **2021**, *403*, No. 126428.
(35) Zhou, D.-D.; He, C.-T.; Liao, P.-Q.; Xue, W.; Zhang, W.-X.; Zhou, H.-L.; Zhang, J.-P.; Chen, X.-M. A Flexible Porous Cu(II) Bis-Imidazolate Framework with Ultrahigh Concentration of Active Sites for Efficient and Recyclable CO_2 Capture. *Chem. Commun.* **2013**, *49*, 11728−11730.
(36) Wu, Y.; Chen, H.; Liu, D.; Qian, Y.; Xi, H. Adsorption and Separation of Ethane/Ethylene on ZIFs with Various Topologies: Combining GCMC Simulation with the Ideal Adsorbed Solution Theory (IAST). *Chem. Eng. Sci.* **2015**, *124*, 144−153.
(37) Wang, Y.; Huang, N.-Y.; Zhang, X.-W.; He, H.; Huang, R.-K.; Ye, Z.-M.; Li, Y.; Zhou, D.-D.; Liao, P.-Q.; Chen, X.-M.; Zhang, J.-P. Selective Aerobic Oxidation of Metal-Organic Framework Boosts Thermodynamic and Kinetic Propylene/Propane Selectivity. *Angew. Chem., Int. Ed.* **2019**, *58*, 7692−7696.

https://doi.org/10.1021/acsami.1c09808
ACS Appl. Mater. Interfaces 2021, 13, 35990−35996

Supporting Information

Propane-Trapping Ultramicroporous Metal-Organic Framework in the Low-Pressure Area toward the Purification of Propylene

Shan-Qing Yang,[a#] Fang-Zhou Sun,[a#] Rajamani Krishna,[b] Qiang Zhang,[a] Lei Zhou,[a] Ying-Hui Zhang,[a] Tong-Liang Hu*[a,c,]

[a] School of Materials Science and Engineering, National Institute for Advanced Materials, Nankai University, Tianjin 300350, China. Email: tlhu@nankai.edu.cn (T.-L. Hu).

[b] Van 't Hoff Institute for Molecular Sciences, University of Amsterdam, Science Park 904, 1098 XH Amsterdam, The Netherlands.

[c] State Key Laboratory of Coordination Chemistry, Nanjing University, Nanjing 210023, China.

[#] These authors contributed equally to this work.

Experimental Section

Breakthrough simulations

The performance of industrial fixed bed adsorbers is dictated by a combination of adsorption selectivity and uptake capacity. Transient breakthrough simulations were carried out for 50/50 and 90/10 alkene/alkane mixtures in **NUM-7a** operating at a total pressure of 100 kPa, and temperatures of 298 K and 313 K, using the methodology described in earlier publications.[1-5] For the breakthrough simulations, the following parameter values were used: length of packed bed, L = 0.3 m; voidage of packed bed, e = 0.4; superficial gas velocity at inlet, u = 0.04 m s^{-1}.

The y-axis is the dimensionless concentrations of each component at the exit of the fixed bed, normalized with respect to the inlet feed concentrations. The x-axis is the dimensionless time, $\tau = \frac{tu}{L\varepsilon}$, defined by dividing the actual time, t, by the characteristic time, $\frac{L\varepsilon}{u}$. The breakthrough simulations demonstrate the potential of producing nearly pure product gas C_3H_6 during the time interval $\Delta\tau$ for both 50/50 and 90/10 C_3H_6/C_3H_8 mixtures.

Notation

L	length of packed bed adsorber, m
t	time, s
T	absolute temperature, K
u	superficial gas velocity in packed bed, m s^{-1}

Greek letters

ε	voidage of packed bed, dimensionless
τ	time, dimensionless

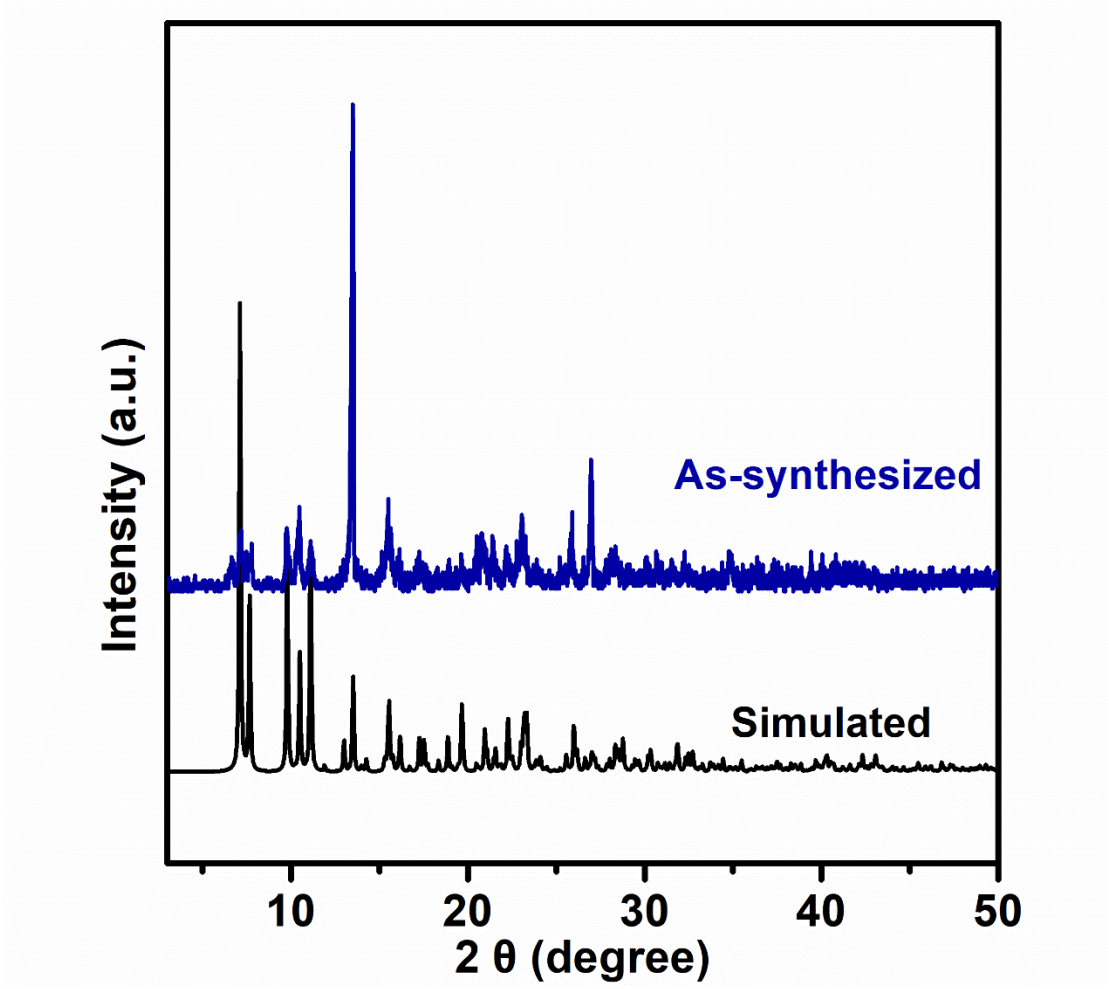

Figure S1. PXRD patterns of **NUM-7**. The experimental result of as-synthesized sample and the simulation from single crystal X-ray diffraction data.

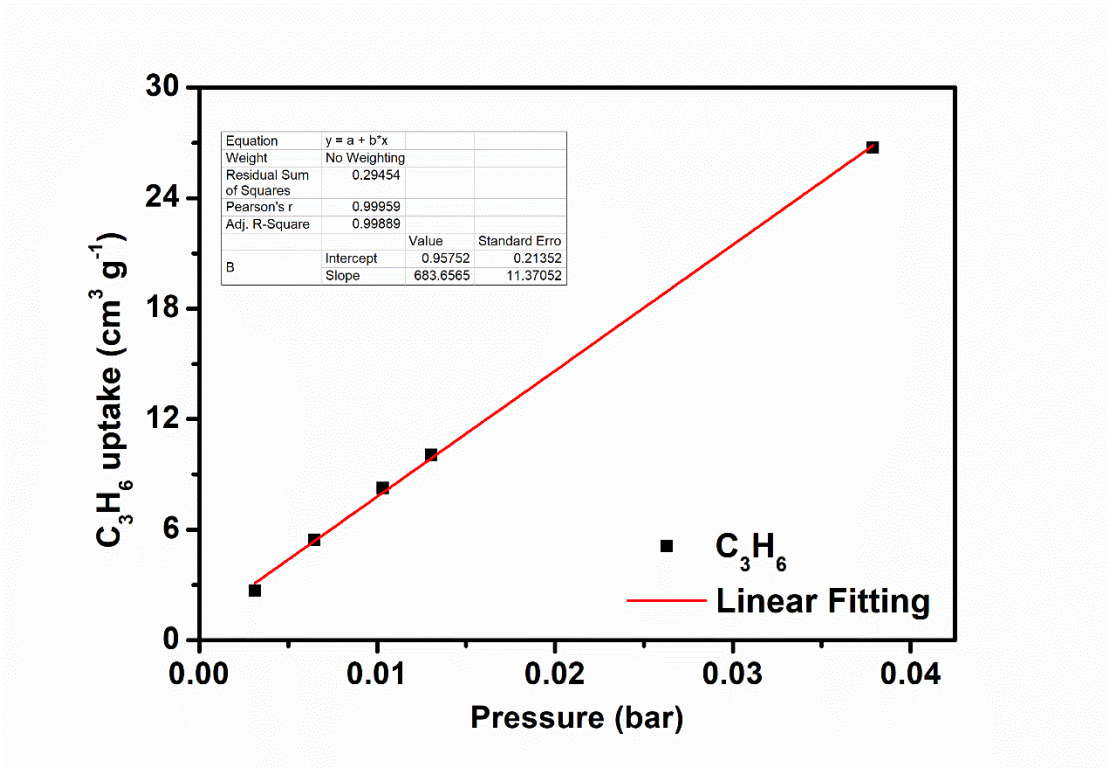

Figure S2. The linear fitting of the C_3H_6 adsorption isotherm in the low pressure for **NUM-7a** at 298 K. The Henry selectivity is the ratio of their slope.

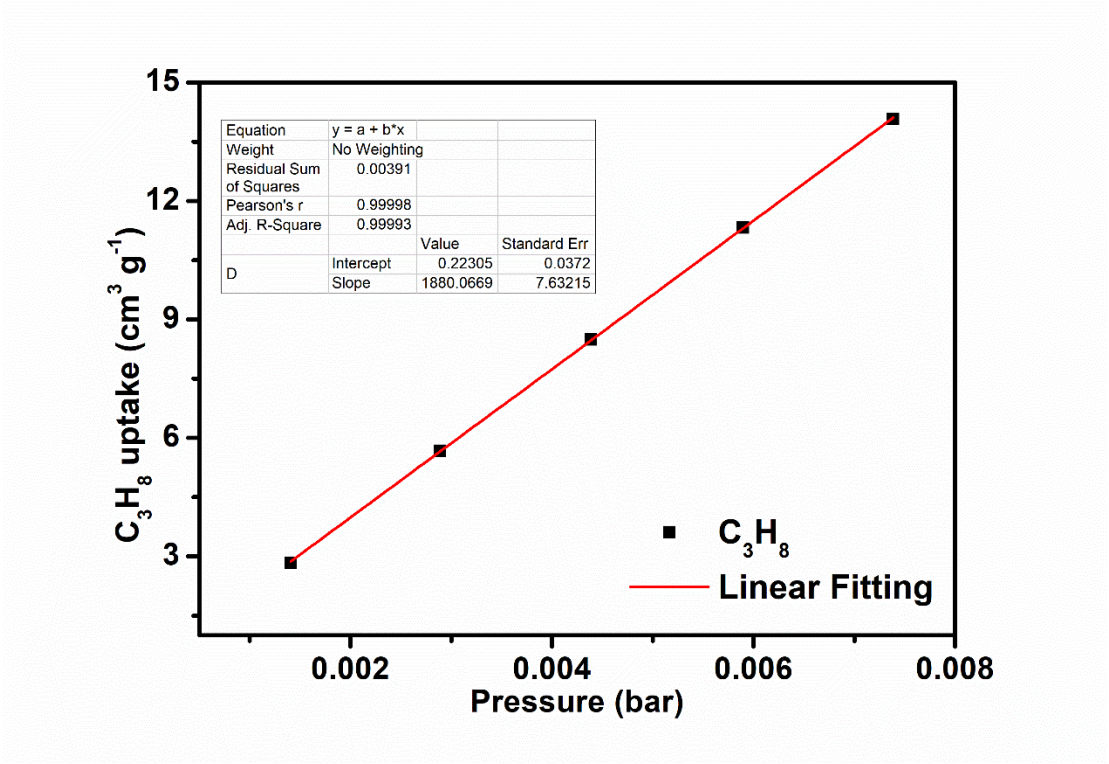

Figure S3. The linear fitting of the C_3H_8 adsorption isotherm in the low pressure for **NUM-7a** at 298 K. The Henry selectivity is the ratio of their slope.

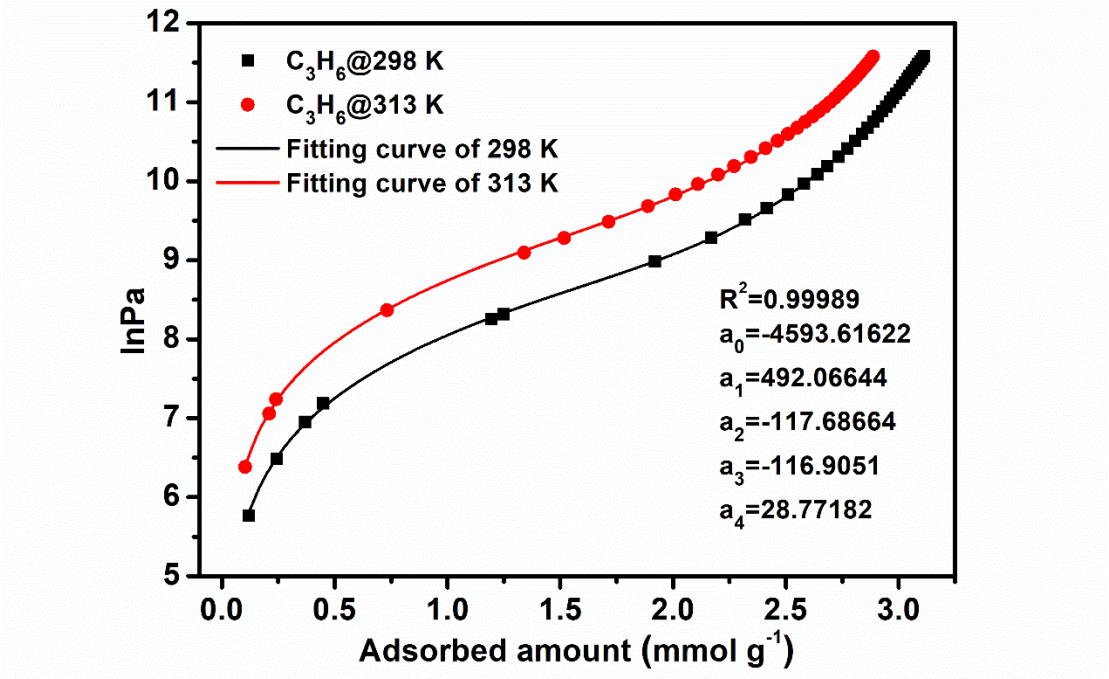

Figure S4. The details of virial equation (solid lines) fitting to the experimental C_3H_6 adsorption data (symbols) for **NUM-7a**.

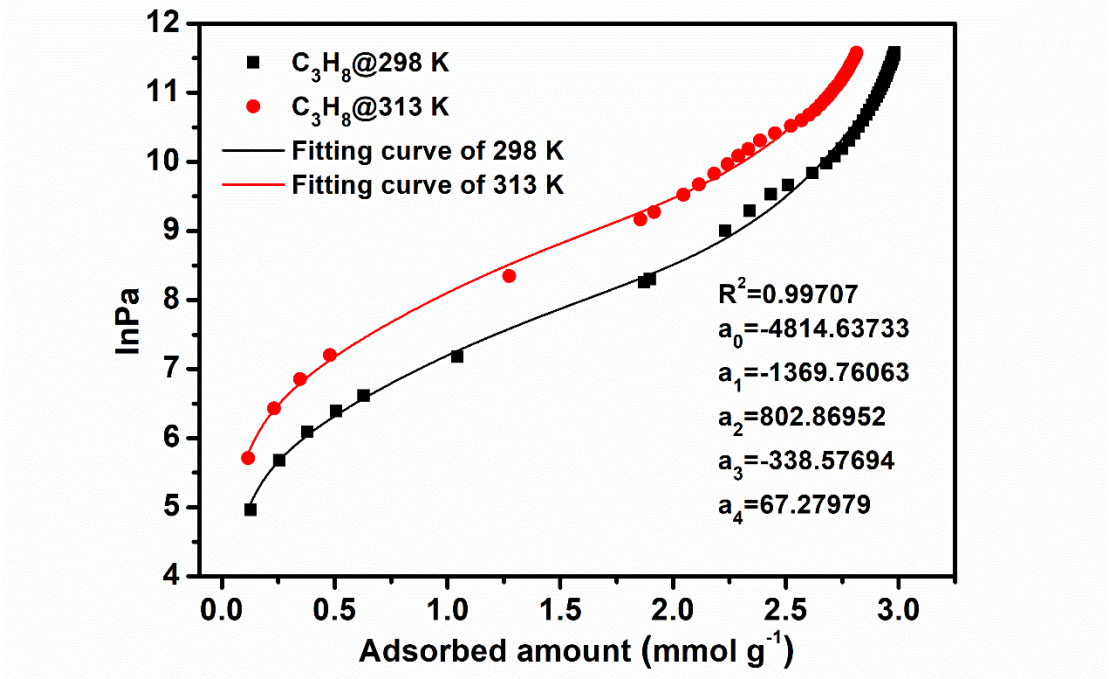

Figure S5. The details of virial equation (solid lines) fitting to the experimental C_3H_8 adsorption data (symbols) for **NUM-7a**.

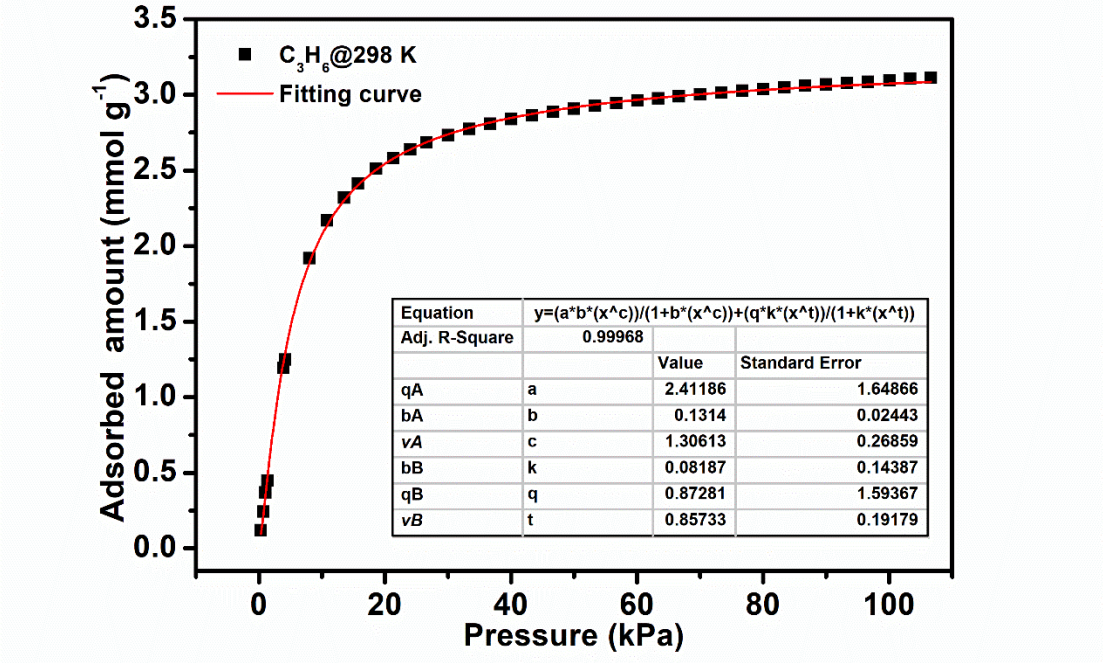

Equation	y=(a*b*(x^c))/(1+b*(x^c))+(q*k*(x^t))/(1+k*(x^t))		
Adj. R-Square	0.99968		
		Value	Standard Error
qA	a	2.41186	1.64866
bA	b	0.1314	0.02443
vA	c	1.30613	0.26859
bB	k	0.08187	0.14387
qB	q	0.87281	1.59367
vB	t	0.85733	0.19179

Figure S6. Dual-site Langmuir-Freundlich model for C_3H_6 adsorption isotherm on **NUM-7a** at 298 K.

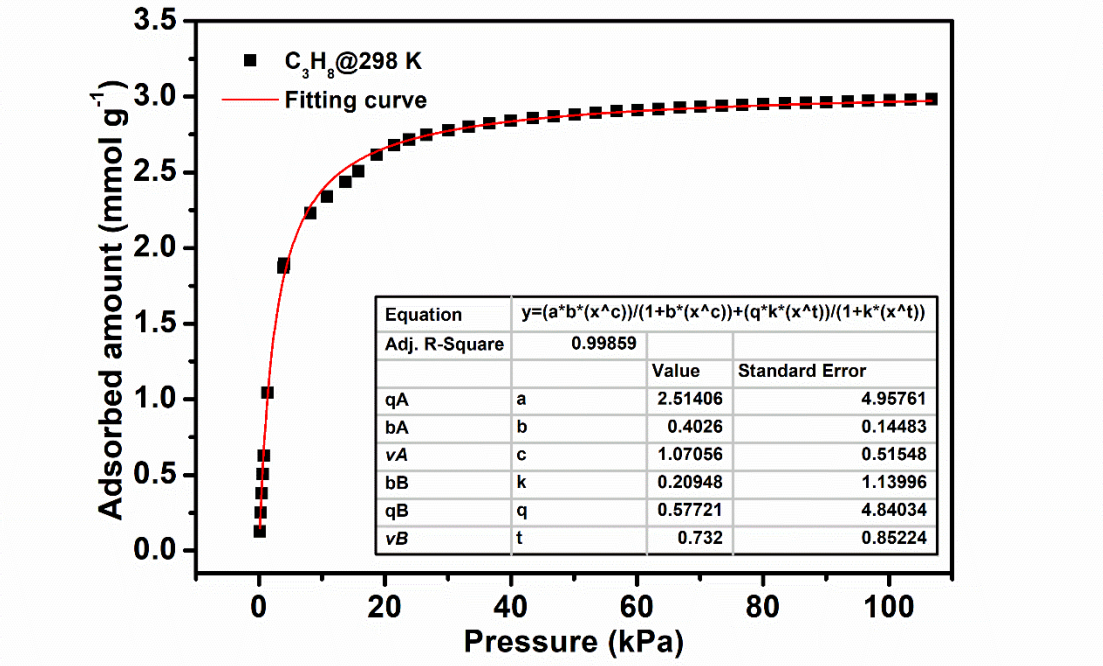

Equation	y=(a*b*(x^c))/(1+b*(x^c))+(q*k*(x^t))/(1+k*(x^t))		
Adj. R-Square	0.99859		
		Value	Standard Error
qA	a	2.51406	4.95761
bA	b	0.4026	0.14483
vA	c	1.07056	0.51548
bB	k	0.20948	1.13996
qB	q	0.57721	4.84034
vB	t	0.732	0.85224

Figure S7. Dual-site Langmuir-Freundlich model for C_3H_8 adsorption isotherm on **NUM-7a** at 298 K.

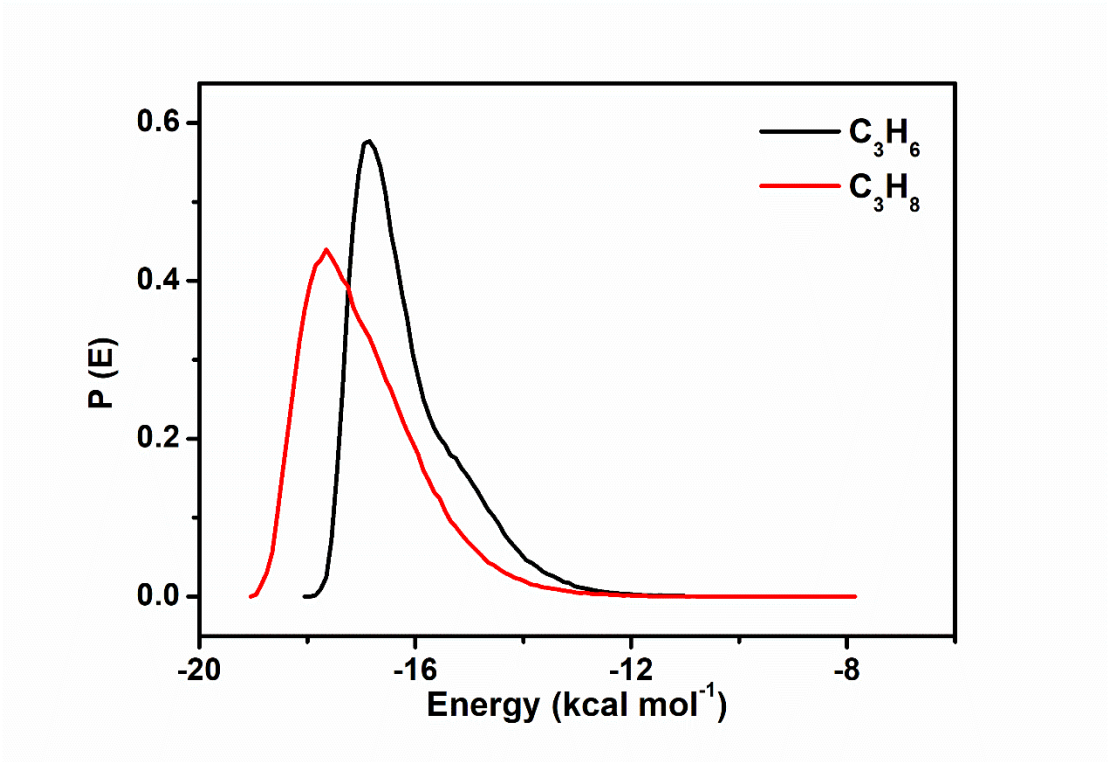

Figure S8. Energy distribution of C_3H_6 and C_3H_8 during adsorption in **NUM-7a**.

References

(1) Krishna, R. The Maxwell-Stefan Description of Mixture Diffusion in Nanoporous Crystalline Materials. *Microporous Mesoporous Mater.* **2014**, *185*, 30-50.

(2) Krishna, R. Methodologies for Evaluation of Metal-Organic Frameworks in Separation Applications. *RSC Adv.* **2015**, *5*, 52269-52295.

(3) Krishna, R. Screening Metal-Organic Frameworks for Mixture Separations in Fixed-Bed Adsorbers using a Combined Selectivity/Capacity Metric. *RSC Adv.* **2017**, *7*, 35724-35737.

(4) Krishna, R. Methodologies for Screening and Selection of Crystalline Microporous Materials in Mixture Separations. *Sep. Purif. Technol.* **2018**, *194*, 281-300.

(5) Krishna, R. Metrics for Evaluation and Screening of Metal-Organic Frameworks for Applications in Mixture Separations. *ACS Omega,* **2020**, *5*, 16987-17004.